https://doi.org/10.5194/egusphere-2025-4263
Preprint. Discussion started: 7 October 2025

Groundwater Maintains Lake Clusters: Groundwater pattern of the Songnen Basin from a Multi-source Remote Sensing Perspective

Xiangmei Liu[1,2], Peng Shen[3], Jiaqi Chen[1*], David Andrew Barry[4], Christian Massari[5], Jiansheng Chen[6], Mingming Feng[7,8], Xi Zhang[9], Fenyan Ma[10], Fei Yang[11], Haixia Jin[1]

[1]*College of Information Science and Engineering, Hohai University, Changzhou 213200, China*

[2]*College of Artificial Intelligence and Automatio, Hohai University, Changzhou, 213200, China*

[3]*Shanghai Aerospace Electronics Co., Ltd., Shanghai, 201821, China*

[4]*Ecological Engineering Laboratory, Environmental Engineering Institute, Faculty of Architecture, Civil and Environmental Engineering, École Polytechnique Fédérale de Lausanne, Lausanne 1015, Switzerland*

[5]*National Research Council (CNR), Research Institute for Geo-Hydrological Protection, Perugia, 06126, Italy*

[6]*School of Earth Science and Engineering, Hohai University, Nanjing 211100, China*

[7]*Key Laboratory of Wetland Ecology and Environment, Northeast Institute of Geography and Agroecology, Chinese Academy of Sciences, Changchun 130102, China*

[8]*University of Chinese Academy of Sciences, Beijing 100049, China*

[9]*Institute of Hydrogeology and Environmental Geology, Chinese Academy of Geological Sciences, Xiamen, 361000, China*

[10]*College of Energy and Power Engineering, Lanzhou University of Technology, Lanzhou, 730050, China*

[11]*Hanggin Banner River and Lake Protection Center, Ordos, 017400, China*

[*]Corresponding author: Jiaqi Chen

Email: jiaqichen@hhu.edu.cn

Abstract

Large-scale lake clusters serve as important freshwater resources in arid and semi-arid regions, but the groundwater recharge patterns sustaining these clusters remain poorly researched. The Songnen Basin, a semi-arid region in northeastern China, contains numerous shallow lakes most of which are not connected to rivers, showing complex interconnections with the groundwater recharge and storage. Here, this paper investigates the role of groundwater in sustaining the freshwater in the lake clusters of the Songnen Basin using remote sensing and isotope analysis, especially during the winter of Chagan Lake, the largest lake in this basin. Our results suggest that deep groundwater upwelling through fault zones is a significant recharge source for Chagan Lake, contributing to the frequent occurrence of stable ice-free areas. Isotopic tracers indicate that this deep groundwater does not originate from local precipitation but likely originates from external sources, potentially the Tibetan Plateau. A deep-circulation groundwater pattern is proposed, suggesting that water-conduiting channels exist under the deep lithosphere in arid and semi-arid regions. When these channels are destroyed by earthquakes, deep-circulating groundwater would rises through faults and recharges lake clusters.

Keywords: Remote sensing, Groundwater, Hydrogen-oxygen isotopes, Songnen Basin

https://doi.org/10.5194/egusphere-2025-4263
Preprint. Discussion started: 7 October 2025

1. Introduction

Currently, approximately 50% of global residential water and 43% of agricultural irrigation are supplied by groundwater, which irrigates 38% of the worlds farmland (Zhang et al., 2021). Abundant groundwater resources are distributed in major plains, intermontane basins, deserts and piedmont plains of inland basins. Groundwater stored in sediment pores, rock fractures, and karst caves, has been a primary target for extraction (Roded et al., 2023;Schilling et al., 2023). Many large plains and basins exhibit artesian characteristics, with confined groundwater levels above the surface, such as the China's Tarim Basin, Qaidam Basin, Hexi Corridor, Ordos Basin, and North China Plain (Liao et al., 2022;Zhang et al., 2021;Li et al., 2024). The Great Artesian Basin in Australia, one of the worlds largest artesian basins, supplies approximately 350 million m^3 groundwater annually through more than 2,000 boreholes (Habermehl, 2006). In the desert and semi-desert regions of Kazakhstan, nearly 70 artesian basins have been identified, covering a total area of 2 million km^2 with a groundwater volume of about 7000 km^3 (Abuduwaili et al., 2018). Rivers and lakes in these artesian basins are recharged by groundwater, serving as crucial water sources for local people (Jiang et al., 2020). However, there remains insufficient research on the recharge, runoff and discharge patterns of groundwater in these regions.

The Songnen Basin, located in northeastern China, is an artesian basin with ten thousands of isolated water bodies (Du et al., 2020). Within this basin, 6,397 water bodies exceeding 60 ha encompass a total area of 432,600 ha sustained by groundwater (Song et al., 2011)(**Fig. 1a-b**). Groundwater is essential for maintaining these water bodies in the semi-arid region, where evaporation greatly exceeds precipitation. When groundwater and runoff recharge decreased in the 1960s, Chagan Lake, the largest lake in this basin (**Fig. 1c**), shrunk by 70% (Wang et al., 2011;Currell et al., 2012) and its pH increased from 8.5 to 12.8 (Lu et al., 2007), threatening water and fish quality. In response to these environmental challenges, the local government initiated the Yinsong Project, constructing Yinsong Channel to connect the Songhua River and Chagan Lake. Unexpectedly, this channel does not transport water from the Songhua River after completion and its headwork has been blocked. Instead, continuous groundwater flows into the channel and has become a vital source for Chagan Lake (**Fig. 1d**).

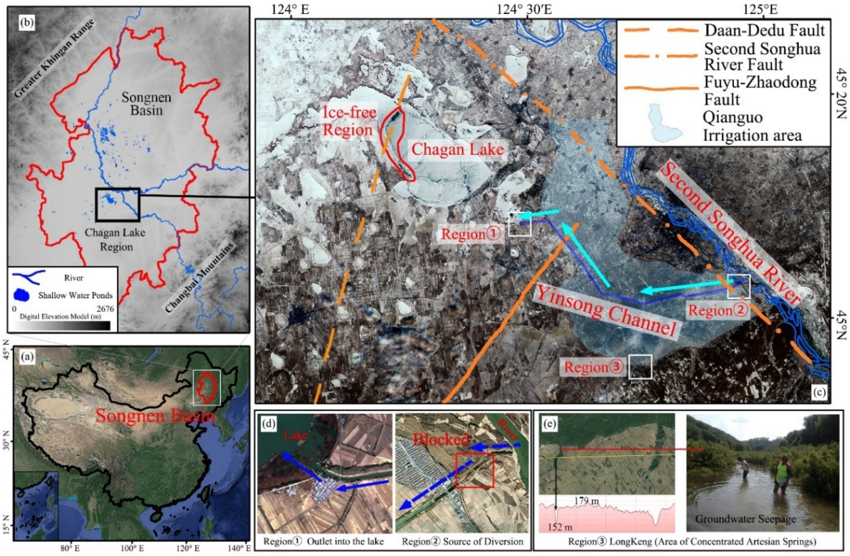

Fig. 1 A map of Chagan Lake region. (a) The Songnen Basin, a major physiographic unit among Northeast Chinas three principal plains, extends north -south and is narrow east-west. Its mean air temperature is about 5°C, varying from -18°C in January to 23°C in July. Annual precipitation and actual evaporation in the basin range from 300 to 600 mm and 1200 to 1800 mm, respectively. (b) Distribution of lake clusters. Chagan lake is the largest shallow lake in the Songnen. (c) Chagan Lake is recharged by Yinsong Channel, and ice-free regions appear on the lake during the winter. Three major irrigation regions are distributed around Chagan Lake, including Daan, Qianan, and Qianguo irrigation regions, encompassing a total area of 5,353.25 km². Among them, the Qianguo irrigation region has the largest area, accounting for 50.36% of the total (d) The Yinsong Channel is an artificial channel extending 53.85 km in length and 50 m in width, connecting Chagan Lake and the Songhua River. After its completion in 1984, the channel has provided an annual water supply of 300 million m³ to Chagan Lake. Landsat imagery reveals that the channels upstream section at the Songhua River confluence has been completely blocked since 1990. (e) The groundwater source of Longkeng region and the field photograph.

The average age of groundwater in the Songnen Basin is only 46.1 years (Zhang et al., 2017), and the recharge, runoff, and discharge patterns of this renewing groundwater are controversial. Previous studies on the groundwater circulation in the Songnen Basin and similar artesian basins have been based on the hydrological water balance, under the assumption that surface water and groundwater within a basin are derived from internal precipitation or inter-basin river recharge, with no cross-basin groundwater recharge (Liu et al., 2017;Chen et al., 2011;Zhang et al., 2015). Notably, despite declining trends in surface runoff and precipitation (Wang et al., 2015), groundwater recharge showed an increasing trend in the Songnen Basin by 2010 (Ma et al., 2021a). In addition to traditional infiltration and lateral recharge, there is also a fault zone recharge mechanism for groundwater (Tan et al., 2021). The Songnen Basin is characterized by numerous fault zones, with lakes and rivers distributed along these faults. Several studies have found that in the Songnen Basin, Changbai Mountains, Greater Khingan Range, and Sanjiang Plain in the Northeast China, the hydrogen-oxygen isotope tracers in groundwater show marked differences with respect to local precipitation, indicating an imbalance in water volume and signs of external groundwater recharge from distant sources to surface water (Zhan et al., 2017;Ma et al., 2021a).

However, the complex hydrological system poses significant challenges in studying groundwater circulation and flow processes in the Songnen Basin, especially when exploring the formation of artesian basins and lake clusters. The groundwater cycle in the basin is influenced by numerous natural and human factors such as precipitation, evaporation, seasonally frozen soil, snowmelt, agricultural irrigation and among others. To minimize the influence of these factors on the groundwater cycle, winter in the Songnen basin has become an ideal period to assess the contribution of external groundwater recharge to this basin. From November to February, seasonal permafrost and snowmelt have not yet begun recharging groundwater, and the total precipitation is only 33.5 mm. During this time, the average air temperature in the Songnen Basin is above -17°C, with ice on Chagan Lake reaching a thickness of up to 1 meter in winter. However, there are some spots and strips shaped areas on the lake where water remains unfrozen or shows thinner ice, suggesting influence of underground springs reaching the surface. The water source of these springs remains unkown, whether it originates from groundwater entering the lake through fault zones or from surrounding phreatic water. The answer to this question is strategic for a sustainable management of the Songnen Basin and is key for a better understanding of the groundwater-surface interactions of semi-arid artesian basins.

Traditional field observations are limited by sparse monitoring networks, and remote sensing provides continuous spatiotemporal coverage. The integration of these two approaches establishes a comprehensive monitoring system for studying hydrological cycles (**Fig. 2**). Hence, this paper focuses on the winter of Chagan Lake region in the Songnen Basin to investigate the groundwater recharge patterns of artesian basins using multi-source remote sensing and isotope techniques. First, MODIS and Landsat imagery are fused to construct the formation processes of winter lake ice, identifying the relationships between spring water, fault zones, and water-conducting structures. Next, interferometric measurements and seismic data are employed to reveal potential groundwater recharge sources and water-conducting media. Finally, external groundwater source origins and deep-circulating groundwater patterns are determined through soil profile and hydrogen-oxygen isotope analysis.

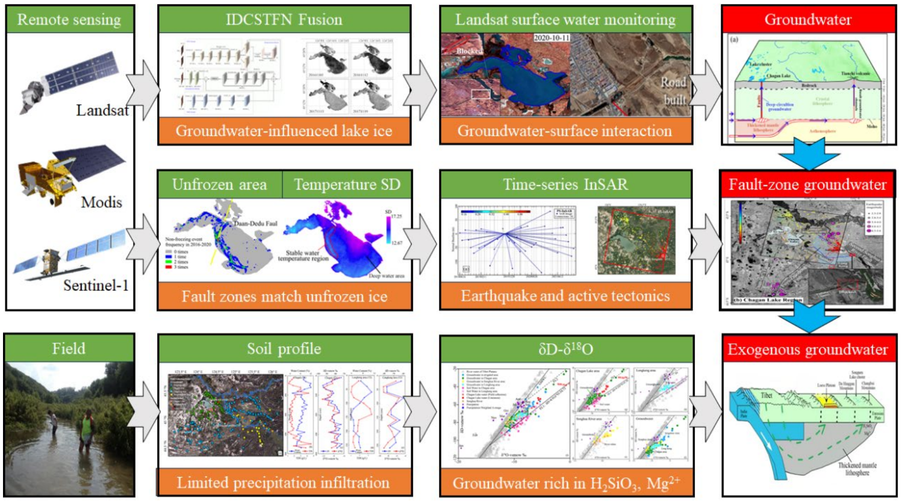

Fig. 2 Flow chart of the groudwater recharge study of Songnen Basin.

2 Results and Discussion

2.1 Chagan Lake region observed by remote sensing

To investigate the groundwater recharge patterns, multi-source remote sensing technology was employed to the Chagan Lake region. We will report our main findings based on three aspects: lake ice formation, Chagan Lake and the Yinsong Channel evolution, and interferometric deformation measurements (**Fig. 3**).

Partial Freezing of Chagan Lake: The ice formation process of Chagan Lake was reconstructed from 2016 to 2020 using the blue band through IDCSTFN. Analysis of **Fig. 3a** reveals that Chagan Lake initiates its freezing process in mid-to-late November annually, typically with an unfrozen area appearing in the northwest region of the lake. As temperatures decrease, this unfrozen region shrinks, and a counterclockwise crack develops along the southwest shore. For example, large unfrozen areas emerged on the lakes western side during the initial ice formation phase in 2016. By mid-November (November 12 and 16), the majority of lake surface had undergone freezing, except for a northeast-southwest-oriented unfrozen area along the southwest shore. Following complete lake freezing on November 20, the pattern persisted with an unfrozen area in the northwest, accompanied by a narrow crack along the southwest shore. Similar cracks or ice ridges aligned with the shoreline appeared in 2018 and 2020. Although similar cracks were not detected in 2017, a large unfrozen

https://doi.org/10.5194/egusphere-2025-4263
Preprint. Discussion started: 7 October 2025

area remained evident in the northwest.

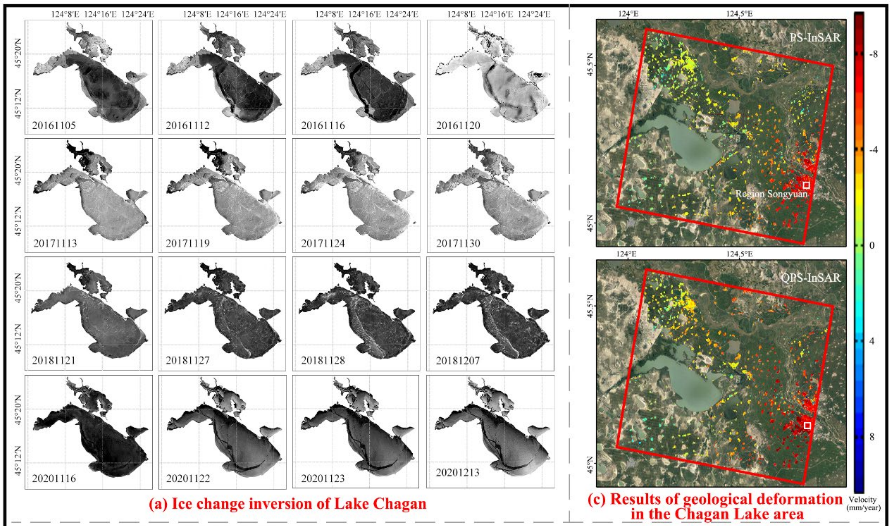

(a) Ice change inversion of Lake Chagan

(c) Results of geological deformation in the Chagan Lake area

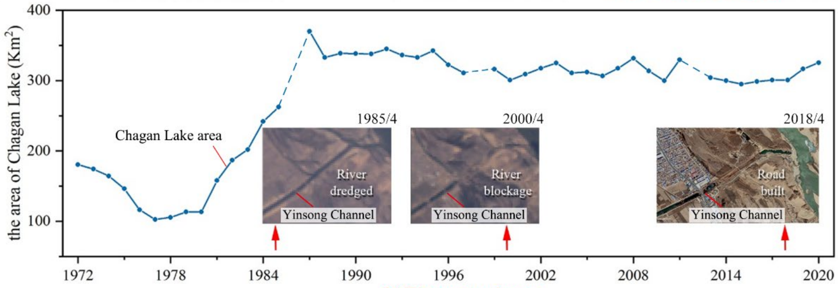

(b) Water area changes

Fig. 3 Changes in lake ice, water area, and surrounding deformation in the Chagan Lake observed by remote sensing. (a) The inversion process of lake ice formation in November for the years 2016, 2017, 2018, and 2020. MODIS and Landsat images were fused to determine the relationship between the springs feeding Chagan Lake and the surrounding water-conducting structures, based on the formation process and spatial distribution of winter lake ice. Landsat and Modis images were fused to reconstruct the lake ice formation from 2016 to 2020, focusing on unfrozen areas (2019 images were missing due to cloud cover) (b) A time series of Chagan Lakes area from 1972 to 2020 was constructed, yielding an overall accuracy of 94.7% and a Kappa coefficient of 0.917. The Kappa coefficient is a statistical measure that evaluates the agreement between classified data and reference data.Due to flood events in 1986, 1998, and 2012, these three years are excluded and are indicated with dashed lines. (c) Deformation measurements around Chagan Lake using PS-InSAR and QPS-InSAR. Synthetic Aperture Radar (SAR) interferometry 23, 24 was employed to analyze surface deformation, integrating earthquake data, water flow distribution, and isotopic characteristics so to identify potential recharge sources and water transmission mediums for groundwater in the Songnen Basin.

Chagan Lake Saved by the Yinsong Channel: The extraction of water bodies was performed using the neural network and Yinsong Channels images were acquired from the corresponding period via Landsat from 1972 to 2020 (**Fig. S1, Fig. 3b**,). During the period 1972-1976, Chagan Lake gradually shrank from 181.9 km² to 118.1

km². To halt this decline, the local government initiated the Yinsong Project, which constructed the Yinsong Channel between the upper Songhua River and Chagan Lake. Following the completion of the first phase in December 1977, water from the Second Songhua River began flowing into the Yinsong Channel. Consequently, the lake s area expanded from 104.9 km² to 246.7 km² during 1977-1984, representing a more than twofold expansion. The completion of the Yinsong Channel's headworks in the second project phase (1984) facilitated a subsequent expansion of Chagan Lake, reaching a total area of 373.9 km² in 1987. Interestingly, the channels head was blocked after 1989, preventing water from the Songhua River flowing into Chagan Lake through the Yinsong Channel (**Fig. 3b**). Nevertheless, a persistent hydrological input recharging Chagan Lake through the Yinsong Channel continues to exist, and the lakes area has remained above 300 km² since 1990.

Subsidence in the Chagan Lake Region: To investigate tectonic activity in the Chagan Lake region, 39 images from 2018 to 2021were selected using PS-InSAR and QPS-InSAR through the SARProz tool (Bai et al., 2022;Perissin et al., 2012). The result identified 13,358 PS points through PS-InSAR and 13,739 points through QPS-InSAR, exhibiting overall coherence greater than 0.8 and similar deformation results In the Songnen region, characterized by densely distributed PS points, the cumulative subsidence measured by PS-InSAR and QPS-InSAR reached 27.44 mm and 25.71 mm (**Fig. S2**). The time-series measurements from both methods demonstrated a high correlation of 0.99, with a deformation error of 1.73 mm. Both methods indicated that subsidence is the primary ground movement in the Chagan Lake region along the line of sight direction (**Fig. 3c**). The subsidence pattern intensifies from west to east, particularly in the Songyuan City and Yinsong Channel region, where the subsidence rate exceeds 7 mm/a.

2.2 Chagan Lake is recharged by fault zone groundwater

The stable ice-free regions of Chagan Lake provide a research target for exploring groundwater sources. The formation of lake ice is influenced by some factors, including temperature, wind, solar radiation, water depth (Dibike et al., 2011). It can be assumed that solar radiation is uniform across the whole Chagan Lake, considering its area only 420 km². Lakes normally begin to freeze at the edges near the land, then expand to the center. And the freezing time is linearly related to the lakes depth, with a delay of one day per meter increasing in depth (Kirillin et al., 2012). The extracted ice-free regions

https://doi.org/10.5194/egusphere-2025-4263
Preprint. Discussion started: 7 October 2025

predominantly occur in the northwest and along the southwestern shore of Chagan Lake, while the deeper central regions typically freeze earlier (**Fig. 4a**), which contradicts the general pattern that deeper waters tend to freeze more slowly. The overlay of these extracted unfrozen regions indicates that the northwest side and southwestern shore are most likely to remain unfrozen (**Fig. 4b**). Notably, the western side of the lake consistently exhibits ice-free zones, with the same area remaining unfrozen on three occasions over a five-year period.

The annual temperature variations of Chagan Lakes surface also corroborate the anomalous distribution of lake ice. Landsat-derived water temperature data were employed to analyze temperature variations from August 2016 to July 2017 (**Fig. S3**). The Landsat images during this period were minimally affected by clouds, enabling a comprehensive depiction of the 12-month temperature variations. As temperatures begin to drop in October, the water temperature near the lakes edges becomes significantly lower than at its center. By early winter (November and December), the deeper southeastern part of the lake has already frozen, but the shallower southwestern shore and northwest side present higher water temperature (**Fig. 4c**). Due to the shallow penetration of optical imagery in water, the retrieved temperature only reflects the lakes surface temperature. As winter temperatures continue to drop, the lakes surface temperature becomes primarily influenced by external factors like air temperature and wind, making such phenomena unlikely to occur in other months.

Coincidentally, the areas with frequent ice formation and higher water temperature correspond to the location of the Daan-Dedu Fault (**Fig. 4b**). The Daan-Dedu Fault, which is the largest fault within the Songnen Basin, runs through Chagan Lake. The reverse fault-fold deformation mechanism of this fault zone exhibits both strike-slip and thrusting movements, providing channels for groundwater to discharge. The Standard Deviation (SD) of lake surface temperature, which has been used to trace groundwater discharge in previous studies (Liao et al., 2022;Mallast et al., 2014;Wilson and Rocha, 2012), was calculated from August 2016 to July 2017. An anomalous band-like pattern characterized by minimal temperature variations exists in the central area of Chagan Lake, away from the deep water zones (**Fig. 4d**). This stable water temperature region corresponds to the last frozen area, coinciding with the trend of the Daan-Dedu Fault.

https://doi.org/10.5194/egusphere-2025-4263
Preprint. Discussion started: 7 October 2025

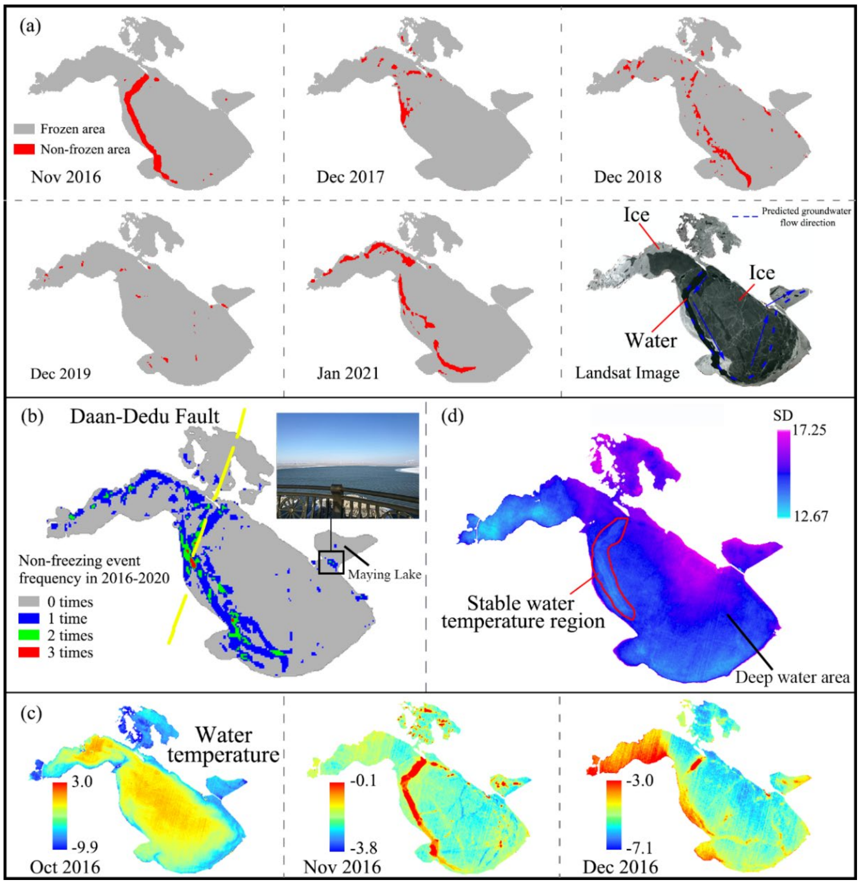

Fig. 4 Inversion results of lake ice and water temperature in Chagan Lake. (a) Extracted results on the non-freezing areas of lake ice from 2016 to 2020 and groundwater flow direction. (b) Frequency distribution of non-freezing events from 2016 to 2020. (c) Inversion results of water temperature from October to December 2016. (d) Standard deviation of water temperature.

The distribution of ice-free areas, SD anomaly zones, and fault zones are consistent, suggesting that warmer deep groundwater likely upwells through the fault, leading to the spatial distribution of water temperature and lake ice. The groundwater from the fault flows west to east towards the Maying Lake, which is a drainage outlet at the northeastern side of Chagan Lake (**Fig. 4b**). Influenced by the Coriolis force, the upwelling groundwater shifts southward, forming a fracture along the southwestern shore of the Chagan Lake (**Fig. 4a**). Since the southeastern part of the lake is in a deep water area (> 4m), the fracture terminates in that direction. Due to the influence of water flow, ice-free regions are observed in the shallower Maying Lake region, consistent with field observations (**Fig. 4b**). The distribution of these regions is also uncertain due to multiple factors such as temperature and wind direction.

2.3 Songnen Basin is widely recharged by fault zone groundwater

Groundwater recharge through fault zones is similarly widespread in other areas of the Songnen Basin (**Fig. 5a**). For example, the Yinsong Channel continuously supplies water to Chagan Lake, even through its source has been blocked (**Fig. 5b**). The channel is primarily located within the Qianguo irrigation district, and traditional studies suggest that it is recharged by irrigation return flow from this region (Dong and Bao, 2009;Tang et al., 2021). The Yinsong Channel was under construction during the winter when the average temperature was above -17°C. The frozen soil layer, which was formed by the low temperature and exceeded 1 m in thickness, blocked both surface water infiltration and irrigation return flow. During the construction, rising springs and quicksand emerged in some sections after the exposure of a 1-meter-thick frozen soil layer. This indicates that besides precipitation infiltration and irrigation return flow, there are other recharge sources for the Yinsong Canal.

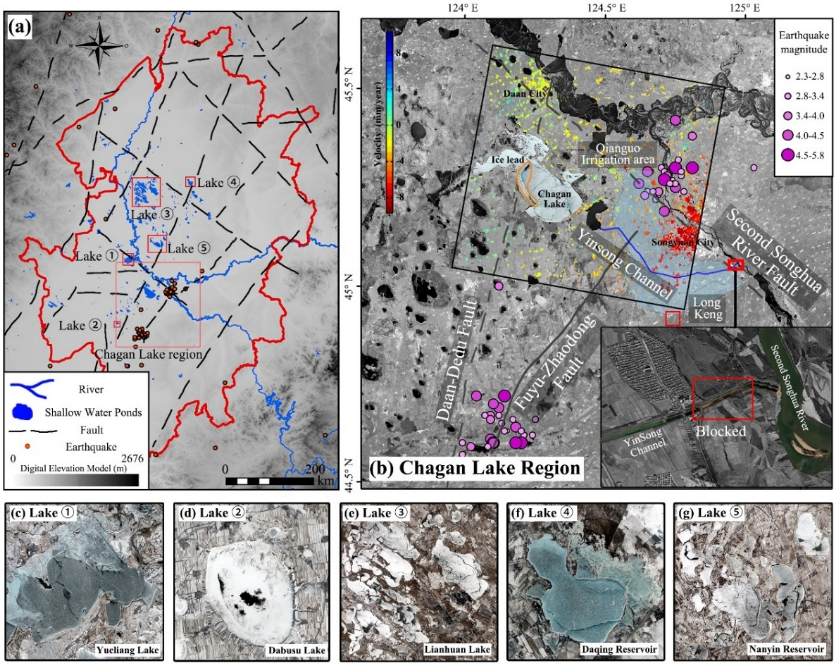

Fig. 5 Distribution map of fault zones and lake clusters in the Songnen Basin. (a) Fault zones, lake clusters, and earthquakes distribution in the Songnen. (b) Deformation measurement results for the Chagan Lake region. The Daan-Dedu, Fuyu-Zhaodong, and Second Songhua River fault zones pass through the Chagan Lake region, with numerous earthquakes occurring on both sides of the fault zones. (c)-(g) are Yueliang Lake, Dubusu Lake, Lianhuan Lake, Daqing Reservoir and Nanyin Reservoir.

Moreover, the inconsistency between water volume fluctuations in the Yinsong

Channel and the irrigation district also suggests the existence of other recharge sources. The annual irrigation return flow in the Qianguo irrigation region was 130 million m^3 from 1975 to 1998, and decreased to 98 million m^3 by 2010, representing a 25% reduction due to water-saving measures(Dong and Hu, 2015). The restoration of Chagan Lake following the Yinsong Channel construction indicates that the channel serves as a vital water source (**Fig. 5b**), contributing 35% of the lakes volume (Zhu et al., 2012). A 25% decrease in irrigation return flow would inevitably affect the Yinsong Channel, potentially leading to the shrinkage of Chagan Lake. However, the Chagan Lake has maintained above 300 km^2, with a recent trend of expansion since 2010.

These two phenomena indicate the Yinsong Channel has additional significant recharge sources besides precipitation and irrigation return flow. Similar to the fault distribution in the Chagan Lake, the north-south trending Fuyu-Zhaodong Fault intersects the Yinsong Channel, and the groundwater discharge from this fault zone becomes a potential recharge source (**Fig. 5b**). Time-series interferences reveal significant subsidence in the Yinsong Channel region at a rate of approximately 4 mm/a. Seismic activities have been concentrated on the eastern side of Chagan Lake since 2013, which coincides with areas of severe subsidence (**Fig. 5b**). The southern section of the Fuyu-Zhaodong Fault is the most seismically active area in Northeast China, with most of the Songnen Basin’s earthquakes concentrated near this fault in recent years (**Fig. 5a**).

The focal depths of these earthquakes range from 4 to 35 km. The largest recorded earthquake in Northeast China occurred in 1119 around the Fuyu-Zhaodong Fault Zone. The earthquake region was located in the Qianguo irrigation area, with a magnitude of 6.75 (Shen et al., 2016). After this earthquake, a substantial volume of groundwater surged from the fault, washing over the overlying loess and formed the Longkeng Gully, located 10 km south of Yinsong Channel (Wu et al., 1988). This natural gully is now approximately 2,500m long, 300m wide and several meters deep (**Fig. 1e**; **Fig. 5**). Numerous rising springs emerge from the Longkeng Gully, forming streams with a stable flow rate of 2m^3/s and a temperature of approximately 10°C. These springs have become a vital water source for the Songyuan city. The existence of Longkeng indicates that frequent seismic activity around the Fuyu-Zhaodong Fault can cause qualitative changes in groundwater movement. Large volumes of groundwater recharge the Yinsong Channel through the fault and eventually flowed into Chagan Lake as the strata subside.

In addition to the Daan-Dedu Fault and Fuyu-Zhaodong Fault, several large N-S and E-W trending fault zones are distributed in the Songnen Basin, including the Nenjiang Fault, Second Songhua River Fault, and Binzhou Fault (**Fig. 5a**). Lake clusters and rivers in the Songnen Basin are situated on a subsidence fault plain formed by these faults. Other lakes in the Songnen Basin, such as Yueliang, Dabusu, Huaao, Xidahai, and Lianhuan lakes, also exhibit unfrozen areas as observed in Landsat images (**Fig. 5c-g**). For example, the Lianhuan Lake region has been developed into a spring resort. These lakes are distributed along fault zones and generally recharged by deep groundwater (**Fig. 5a**). The Songhua and Nenjiang rivers are also aligned with fault zones, which exert a significant influence on the formation and hydrological control of these rivers and lakes.

The NE-SW, NW-SE, and E-W trending fault structures shape the spatial pattern of lake development, and define fault-controlled basins. As analysed by the Dabusu Lake profile near Chagan Lake, the sediments of lakes in the Songnen Basin primarily consist of aeolian deposits and biological remains. The average sedimentation rate of lakes in the Songnen Baisn has been approximately 0.54 mm/a over the past 15000 years (Shen et al., 1998). The Songnen Basin is seismically active, with the eastern region experiencing an average subsidence rate of 4 mm/a (Lingyun et al., 2014). The surface subsidence rate in the Songnen Baisn is significantly higher than the lake sedimentation rate, suggesting that lake evolution is primarily influenced by tectonic displacement rather than sedimentation. Several caves exist within active geological structures, and their collapse leads to surface subsidence. These caves serve as conduits and storage spaces for groundwater. Under the influence of seismic and other geological activities, groundwater from fault zones rises to recharge these shallow lakes, thereby influencing the formation of lake ice.

2.4 Limited local precipitation recharge of fault zone groundwater

Lake clusters in the Songnen receive recharge from fault zone groundwater. And traditional water balance theory suggests that groundwater recharging shallow lakes is derived from precipitation infiltration in surrounding mountainous and plateau areas, or irrigation return flows. If precipitation or irrigation water indeed recharges groundwater through infiltration, it would inevitably lead to soil water saturation. Hence, soil drilling and hydrogen-oxygen isotope measurements were performed during 2017 and 2018 in the Songnen Basin to identify the groundwater sources,

https://doi.org/10.5194/egusphere-2025-4263
Preprint. Discussion started: 7 October 2025

especially the Chagan Lake region.

The locations of the soil profiles includes the Chagan Lake surrounding region (T1), Longkeng region (T2), and Dabusu region (**Fig. 6a**). The maximum water holding capacity of the Dabuxun profile is 13.4% and 14% (**Fig. S4**). This result indicates that the maximum field soil-water holding capacity is ≥14% in the Chagan Lake region due to the relatively uniform granularity of loess. The maximum values of water contents in Profile T1 and T2 are only 12.02% at 120cm and 11.01% at 60 cm below the surface. These values are less than the maximum water holding capacity (14%), indicating a soil moisture deficit (**Fig. 6b-e**).

The Total dissolved solids (TDS) in the Profile T1 around Chagan Lake exhibits two peaks: the first peak occurs at 1.8m with 4.2 g/L, and the second reaches 4.6 g/L at 7.0m. These peaks represent the depth of previous precipitation infiltration. The first peak is influenced by precipitation infiltration, which has transported surface salts into the soil. The secondary peak is related to irrigation or surface water infiltration. This profile is located in a low-lying area where surface water converges, so this location serves as an optimal observation point if groundwater is recharged through soil infiltration. In the Chagan Lake region, the TDS of phreatic groundwater is 0.37-2.1 g/L, with an average of 0.96 g/L. For confined water, TDS is 0.35-1.43 g/L, with an average of 0.6 g/L (Xu et al., 2020). The secondary peak demonstrates that the depth of soil infiltration reaches 7m, with soil water TDS (>4 g/L) exceeding that of groundwater. This peak reflects the depth of surface water infiltration, suggesting limited potential for surface irrigation water to infiltrate into groundwater, even in pothole regions. In the Profile T2 at Longkeng region, the peak TDS occurs at 1.4m, measuring 4.65g/L, which exceeds the maximum TDS of groundwater. Therefore, the previous point that groundwater only originates from local precipitation, irrigation water, and river water infiltration is inconsistent with the sampling results in the Chagan Lake region.

https://doi.org/10.5194/egusphere-2025-4263
Preprint. Discussion started: 7 October 2025

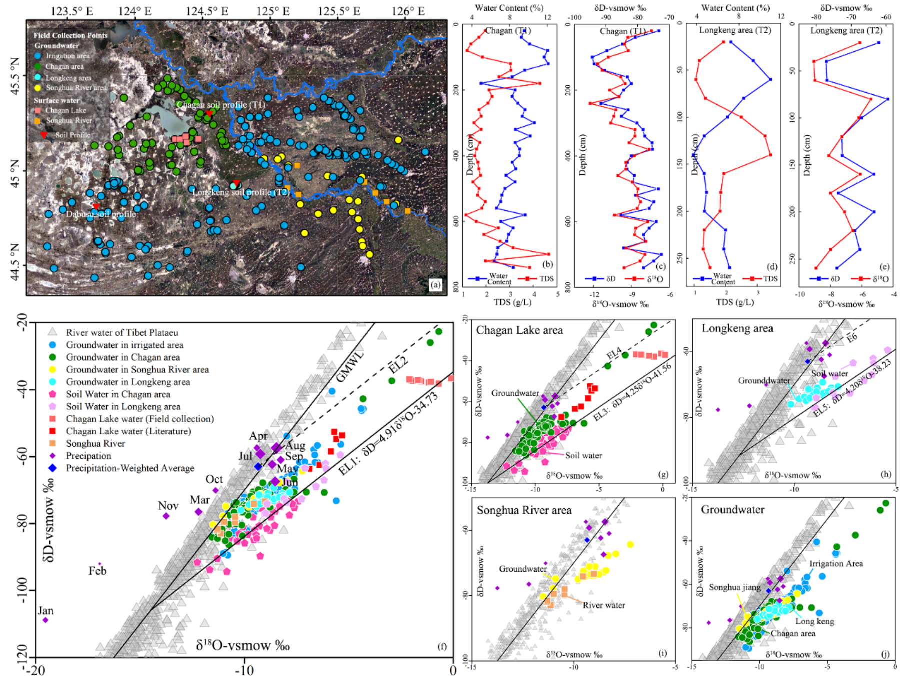

Fig. 6 Field sampling results in the Chagan Lake region. (a) Location map of hydrogen-oxygen isotope and soil profile sampling points. Surface water and groundwater are represented by circles and squares, respectively, and are distinguished by different colors based on the sampling regions. The sampling locations of Chagan, Longkeng, and Dabusu soil profiles are marked by inverted triangles. (b)-(e) TDS, water content, and hydrogen-oxygen isotope results from soil profiles around Chagan Lake (T1) and Longkeng (T2) regions. (f)-(j) Relationships between hydrogen-oxygen isotopes in surface water, soil water, and groundwater in the Chagan Lake region. Groundwater, soil water, surface water, and precipitation are represented by circles, pentagons, squares, and diamonds, respectively. River water from the Tibet Plateau is represented by gray triangles. The isotope characteristics of the collected lake water are almost parallel to the δ^{18}O axis, because the sampling area in Chagan Lake is near the shore, where lake water has low mobility and high evaporation. MuRong Li et al conducted isotope measurements across the entire Chagan Lake in 2019-2022 (Li et al., 2023), and these results were added as literature. EL1-6 are evaporation lines. EL1 represents the evaporation line of soil water in the Chagan Lake and Longkeng regions, while EL3 and EL5 represent the evaporation lines of soil water in the Chagan Lake and Longkeng region, respectively. EL2, EL4, and EL6 are three other lines parallel to the precipitation-weighted average.

The hydrogen-oxygen isotope results also corroborate the conclusion that groundwater has other recharge sources, possibly from extra-basin water. Isotope points were established based on groundwater and surface water samples collected from Chagan Lake, Songhua River, Longkeng, and irrigation regions (**Fig. 6f**). Lake water exhibits greater isotopic enrichment compared to groundwater and soil water. The hydrogen-oxygen relationship points of soil water from Chagan Lake and Longkeng profiles plot along the evaporation line EL1, which differs significantly from local precipitation. Soil water is more depleted than local precipitation points and

https://doi.org/10.5194/egusphere-2025-4263
Preprint. Discussion started: 7 October 2025

precipitation that infiltrates the soil and undergoes evaporation should align with EL2. Therefore, the primary source of soil water is not precipitation. The isotopic characteristics of soil water fluctuate significantly with depth in the Longkeng profile. This profile was sampled in November 2017, after four irrigation events from spring to summer. The soil water enriches in isotope character due to evaporation and transmits deeper after each irrigation, consequently leading to isotope fluctuations. Moreover, the soil water is more enriched than groundwater overall in the Longkeng region, indicating that the soil water originates from groundwater irrigation. Soil water shows greater isotopic depletion relative to groundwater in the Chagan Lake region because it is further from the Global Meteoric Water Line (GMWL) and predominantly affected by evaporation. The irrigation with groundwater, combined with the evaporation-crystallization process, results in further depletion of the soil water.

The hydrogen-oxygen isotopic composition in groundwater, which recharges the soil water, shows more depleted than local precipitation. This isotopic signature indicates that groundwater recharge originates from external sources rather than soil water and local precipitation. The Second Songhua River follows the fault zone and flows through the Chagan Lake region. The isotopic results show that river water is generally more depleted than groundwater, making it a potential source of groundwater recharge (**Fig. 9i**). But topographical constraints preclude it from being a recharge source. The water level of Second Songhua River is 132m in the south and 121m in the north, while the elevation of Longkeng spring is 150m. This significant elevation difference, coupled with the fact that spring water flows into the Second Songhua River, demonstrates that the river water cannot recharge the Fuyu-Zhaodong fault through the Second Songhua River fault.

The Changbai Mountains and Greater Khingan Range, situated on the eastern and western sides of the Songnen Basin, have average elevations exceeding 1000m and significant hydraulic gradients, making them potential groundwater recharge areas for Songnen (Jiang and Chen, 2015;Ma et al., 2021b). However, both regions exhibit water imbalances and receive external groundwater recharge themselves. The Changbai Mountains contribute an average runoff of 3.1×10^{10} m^3, accounting for 87% of Jilin Province's total runoff. But water balance and isotopic analyses reveal that the Tianchi Lake in Changbai Mountain receives external groundwater recharge ($\geq 0.8 m^3/s$) (Jiang and Chen, 2015). In the Greater Khingan Range, deep groundwater discharges through the Erbugan fault and Xinlin-Xiguitu fault zones, resulting in unfrozen rivers in the

Huma River basin even at temperatures of -40°C (**Fig. S5**). Similar to the Songnen Basin, the hydrogen-oxygen isotopes in groundwater from both the Changbai Mountains and Greater Khingan Range are more depleted compared to local precipitation, and the groundwater isotopic compositions of all three regions are similar to rivers in the Tibetan Plateau (**Fig. 6j**).

2.5 Groundwater pattern of artesian basins

The Songnen Basin is characterized by extensive Cenozoic basalts. Recent studies have revealed the existence of a deep-circulation groundwater pattern in areas dominated by Cenozoic basalts. The endorheic region in the Tibetan Plateau loses approximately 540×10^8 m^3 water annually, equivalent to the Yellow Rivers annual flow (Yong et al., 2021). This water is transported to eastern China in the form of deep-circulating groundwater through seepage channels within north-south trending rift valleys of the Tibetan Plateau (Liu et al., 2023). These channels originated as contraction joints formed during the cooling of basaltic magmatic rocks. Numerous artesian basins are situated in the arid and semi-arid regions surrounding the Tibetan Plateau, including the Tarim, Qaidam, Ordos, North China Plain, and Songnen Basin (Ma et al., 2021a;Liu et al., 2024;Chen et al., 2012). There has been considerable attention on whether a potential relationship exists between the Tibetan Plateau' lost water and artesian basins' external groundwater. If these artesian basins receive groundwater recharge from Tibetan Plateau seepage, cooling contraction joints from past magmatic activity must exist between the plateau and these basins. This indicates that since the Cenozoic era, these basins experienced magmatic activity originating from Tibets asthenospheric mantle.

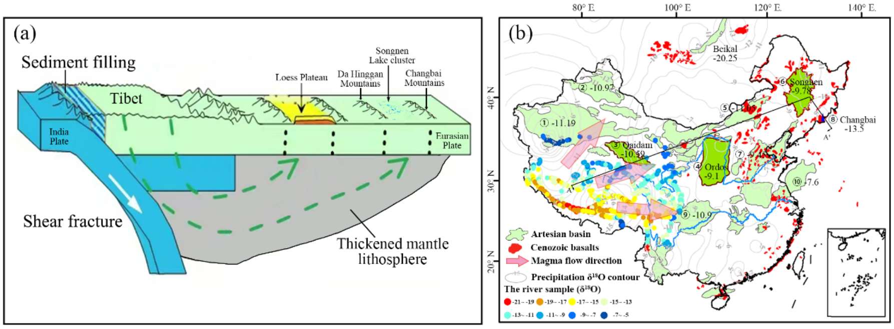

Fig. 7 Conceptual model and distribution of deep circulation groundwater recharge. (a) Conceptual diagram of deep circulating groundwater recharge to lakes and volcanic crater lakes through fault zones (Wang et al., 2025). (b) Distribution of artesian basins, Cenozoic basalts and δ ^{18}O isotopes (Zhang et al., 2025). ①–⑩ correspond to Tarim, Junggar, Qaidam,

Ordos, Erenhot, Songnen, North China Plain, Changbai Mountain, Sichuan, and Subei Basin, respectively.

An estimated 500,000 km³ of freshwater and low-salinity water exists beneath the continental shelves near Australia, China, North America, and South Africa (Post et al., 2013). Traditional groundwater circulation theory suggests this water originated from glacial-period precipitation when sea levels were substantially lower. However, the origin of freshwater and low-salinity water in continental shelf aquifers remains debated, particularly due to the artesian characteristics of submarine freshwater aquifers. Groundwater discharge in the South Atlantic Bay coastal areas amounts to approximately 40% of river discharge, analyzed using 226Ra data from brackish groundwater and coastal water residence time (Moore, 1996). Similarly, substantial freshwater discharge occurs through submarine groundwater along Chinas coastline (Wang et al., 2021). Since glacial-period paleowaters trapped in aquifers lack sustained artesian characteristics, its inferred that continental shelf freshwater originates from deep-circulating groundwater. This is supported by widespread volcanic activity in eastern China during the Cenozoic era, where magmatic flows caused by the subduction of the Indian plate flowed and erupted in three directions: northeast, east, and southeast (**Fig. 7b**). These magmatic flows created water-conducting channels, forming groundwater networks.

Research shows that the Qaidam Basin, adjacent to eastern Tibetan Plateau, receives external water recharge from Tibets endorheic region, and this water upwells to lake clusters through basement fault zones in the basin (Liu et al., 2024). In the eastern Ordos artesian basin, on the top of Lvliang Mountain (2783m), there exists rising springs and lake clusters, which are derived from Tibetan seepage water as measured by hydrogen-oxygen isotope (Zhang et al., 2025). Deep-circulation groundwater from Tibetan recharges the Loess Plateau, where the groundwater penetrating through the lithosphere facilitates the formation of red clay layer (Wang et al., 2025). Based on previous deep circulation groundwater models, this paper constructed a deep-circulating groundwater model for arid and semi-arid regions (**Fig. 7a**). The Indian Ocean plate subducts beneath the Eurasian plate, causing high-pressure in the mantle and triggering volcanic eruptions and magmatic activity. Following the cessation of volcanic eruptions and transition to extinction, the magmatic activity in the mantle ceases, and the magma crystallizes into solid rock masses through thermal equilibration with the adjacent country rocks. The low SiO_2 content in basaltic

https://doi.org/10.5194/egusphere-2025-4263
Preprint. Discussion started: 7 October 2025

magmatic rocks results in reduced magma viscosity, leading to the formation of continuous cooling-contraction fractures along the flow orientation within the basaltic unit. These fractures serve as preferential pathways for rapid groundwater transport between recharge zones and artesian basins (Wang et al., 2024).

Research has revealed that groundwater contributes approximately 65% of the water in the Changbai Mountain Tianchi (Jiang and Chen, 2015). Given Tianchi Lakes elevation of 2,189.7 m, hydraulic and isotopic analyses indicate that Tianchi receives seepage water from Tibet, and there exists water-conducting channels between Tibet and Changbai Mountain. If deep-circulating groundwater recharge reaches the Changbai Mountain, some water-conducting channels must have passed through the Songnen Basin, which is situated between the Tibetan Plateau and Changbai Mountain. Due to seismic activity in Songyuan and its surrounding areas, groundwater upwells through fault zones after the disruption of some water conduits and overflows as springs to form shallow lakes. In these shallow lakes such as Chagan Lake, unfrozen regions during winter are the spring outflow points. An increasing number of studies have revealed that artesian basins in arid and semi-arid regions exists similar groundwater recharge pattern, including the Tarim Basin, Zhangye Basin, Badanjilin Desert, Erenhot Basin, and Hulun Lake Basin (**Fig. S6**). Similar cross-basin recharge exists between numerous sub-basins in the United States, and lateral groundwater recharge distances exceed 200 km in the arid western regions (Yang et al., 2025). The Qiangtang-Songnen deep-circulating groundwater recharge pattern may be widespread in many artesian basins.

2.6 Limitations of the study

Remote sensing and isotope analyses are employed to explore groundwater patterns in the Songnen Basin. However, some limitations still exist, including: (1) Given that the Songnen Bains is situated over 3,000km away from the endorheic Tibetan Plateau, and considering that the water conduit extends to mantle depths, additional comprehensive investigations are required to establish the potential connection between these two regions. (2) The dense vegetation coverage surrounding the Chagan Lake results in a sparse distribution of interferometric points, with high-coherence PS points predominantly concentrated in urban areas, villages, and other built-up areas. Future studies should consider SAR images of different bands or alternative interferometric techniques to mitigate the vegetation-induced impacts on

https://doi.org/10.5194/egusphere-2025-4263
Preprint. Discussion started: 7 October 2025

interferometric results.

3 Conclusion

This paper focuses on the Songnen Basin in the winter to explore the groundwater cycle patterns of the arid and semi-arid artesian basins, using multi-source remote sensing and hydrogen-oxygen isotope techniques. Groundwater from fault zones recharges lake clusters and influences spatio-temporal distribution of lake ice in the Songnen Basin. Contrary to traditional water balance theories, this groundwater does not originate from local precipitation but from external sources. The annual leakage water from the Tibetan endorheic regions is equivalent to the runoff of Yellow River. This leaked water recharges numerous artesian basins through fault zones, including the Qaidam Basin, Ordos Basin, and Changbai Mountains, as well as the Songnen Basin, all along the recharge pathway. Due to limitations in detection technology, there is still insufficient evidence to confirm that this external groundwater originates from the endorheic Tibetan Plateau. Further research is necessary to establish the connection between endorheic Tibetan Plateau and these artesian basins.

4 Material and method

4.1 Data

4.1.1 Remote sensing data

The satellites data utilized in the paper were primarily acquired from Landsat, MODIS and Sentinel-1 (**Table S1**). The Landsat series of satellites, developed by NASA and USGS, have provided Earth observation imagery since 1972 (https://glovis.usgs.gov). This paper primarily utilized Landsat 8 images, with a spatial resolution of 30m and a revisit period of 16 days. MODIS is a satellite sensor jointly developed by NASA and the Committee on Earth Observation Satellites, from which MOD11A1 and MOD09GA data were primarily applied. Landsat and MODIS imagery were mainly employed to analyze lake ice characteristics and observe changes in the Chagan Lake and Yinsong Channel since 1972. The Sentinel-1 constellation comprises Sentinel-1A and Sentinel-1B, launched in 2014 and 2016, respectively. Single Look Complex data acquired from Sentinel-1B in Interferometric Wide mode were used for interferometric measurements to quantify subsidence in the Chagan Lake region.

4.1.2 Water Surface Temperature Retrieval

Based on the Google Earth Engine, the water temperature of Chagan Lake was inverted using USGS Landsat Collection-2 Surface Temperature dataset (Jimenez-

https://doi.org/10.5194/egusphere-2025-4263
Preprint. Discussion started: 7 October 2025

Munoz et al., 2014). This dataset employs atmospheric correction methods to retrieve land-water surface temperatures. Compared with field measurements from seven ground stations, the analysis of 259 satellite images exhibited a mean bias of -0.267°C (Cook, 2014). Liu Xuemei et al. conducted in-situ water temperature measurements of Chagan Lake from 2018 to 2019 (Liu et al., 2020). The Landsat-derived water temperature of Chagan Lake exhibited a correlation coefficient of 0.89 and an error of 1.5°C (**Fig. S7**), when compared with in-situ measurements. The higher error is attributed to temporal mismatches between Landsat image acquisition and in-situ measurements, necessitating the use of temporally proximate images for validation. Nevertheless, the high correlation indicates that this dataset adequately represents the spatial distribution patterns of Chagan Lakes water temperature.

4.1.3 Soil profile sampling and hydrogen-oxygen isotopes

The Qianguo irrigation area has an average annual irrigation return flow of approximately 1.3×10^8 m^3 (Ge et al., 2023), which is condersided crucial for maintaining groundwater levels coupled with precipitation. To evaluate the potential groundwater recharge from precipitation and irrigation water, soil profiles were excavated at three locations in the Chagan Lake, Longkeng, and Dabusui regions. Bulk soil samples were collected using a specialized soil auger at 20-cm depth intervals. Samples were sealed in airtight polyethylene bottles, transported and stored under refrigeration. Soil water was extracted using an automated vacuum condensation extraction system (LI-2100). The extracted soil water was analyzed for δ^2H and $\delta^{18}O$ using a MAT253 mass spectrometer.

Soil water content was determined using the oven-drying method with an analytical precision better than 1%. The frozen soil samples were weighed initially, heated at 110℃ for 3 hours, and reweighed after drying to determine water content. 30g oven-dried soil was mixed with 150 mL of deionized water and equilibrated for 48 hours, followed by centrifugation and filtration. The filtrate was analyzed by a multi-parameter water quality analyzer and ion chromatograph (ICS-2000, Dionex, USA). Ion concentrations in soil water were converted based on the soil moisture content.

In addition to soil profile sampling, 664 water samples from groundwater, river water, and lake water were collected in the Chagan Lake region during 2017 and 2018. The hydrogen and oxygen isotopic compositions ($\delta^{18}O$ and δD) were analyzed using a MAT253 mass spectrometer with analytical precisions of ±0.1‰ and ±2‰, respectively.

4.1.4 Lake Ice Fusion Dataset

This paper integrates Landsat 8 and MOD09GA imagery to build an image fusion dataset and construct the lake ice formation process. Images with cloud cover below 5% underwent radiometric calibration, geometric correction, and atmospheric correction. Landsat images were cropped to 3200×3200 pixels, while MODIS images were resampled to 480m resolution and subsequently cropped to 200×200 pixels. The preprocessed data were organized into groups, with each group containing four images: one pair of temporally coincident MODIS and Landsat images for the prediction date, and one pair of MODIS images temporally adjacent to the prediction date. Through this preprocessing, filtering, and grouping procedure, a dataset containing 21 data groups was established. Among these, 15 groups of images acquired from January 2015 to December 2018 were allocated to the training set, and images acquired from January 2020 to March 2021 were designated as the validation set. The constructed training and testing datasets will provide data for the subsequent training of the Landsat and MODIS fusion model.

4.2 Method

Traditional hydrochemical isotope methods exhibit limitations due to ambiguity in groundwater source tracing. Hence, this paper combines remote sensing (Landsat, MODIS, and Sentinel-1) data and field data (soil profile and hydrogen-oxygen isotopes) to investigate the groundwater recharge pattern in the Songnen Basin. We will introduce our main methods used for lake ice inversion and deformation measurement in the following sections.

4.2.1 IDCSTFN fusion of Landsat and MODIS

To continuously and stably monitor the lake ice characteristics of Chagan Lake and analyze groundwater discharge areas, this paper employs an Improved Deep Convolutional Spatiotemporal Fusion Network (IDCSTFN) to fuse Landsat and MODIS imagery. This method combines Landsats high spatial resolution with MODISs high temporal resolution to construct the lake ice formation sequence . The traditional DCSTFN follows the principles of the Spatial and Temporal Adaptive Reflectance Fusion Model (STARFM), which assumes that surface conditions remain nearly identical between reference and prediction dates. However, this assumption cannot adequately address the rapid ice growth in the Lake Chagan region.

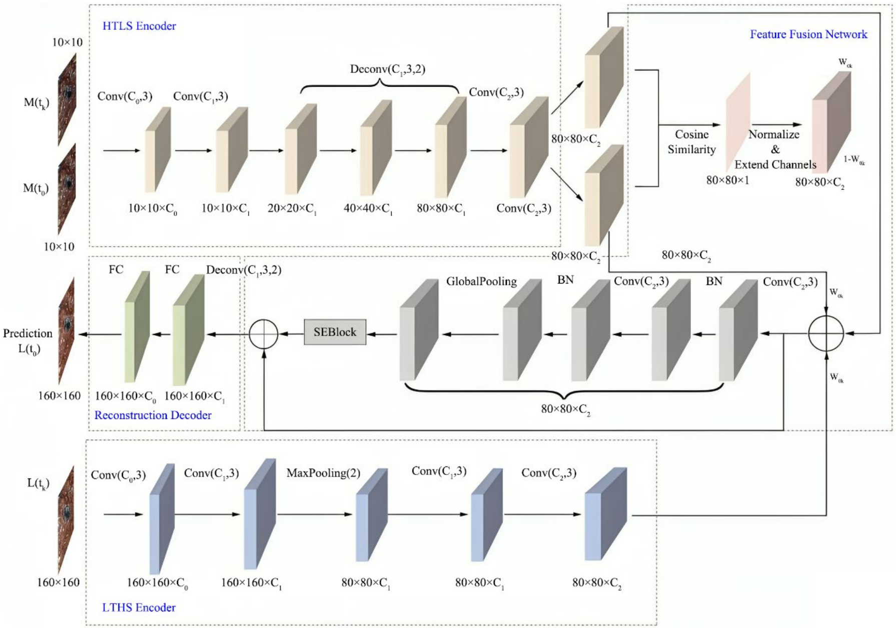

Fig. 8 IDCSTF structure diagram.

Therefore, IDCSTFN utilizes a feature fusion network to replace the assumption equations in DCSTFN. The proposed fusion network computes the differences between reference and predicted images as weights to fuse input images, and subsequently employs attention residual blocks to eliminate redundant features, enhance key features of fused images, and prevent overfitting (**Fig. 8**). IDCSTFN implements an "encoder-fusion-decoder" architecture, comprising four main modules: the High Temporal but Low Spatial (HTLS) encoder, Low Temporal but High Spatial (LTHS) encoder, feature fusion, and reconstruction decoder. The network culminates in two successive fully connected layers that reduce the dimensions of the fused feature map, generating in a high-resolution fused image (specified in the supplement, IDCSTFN).

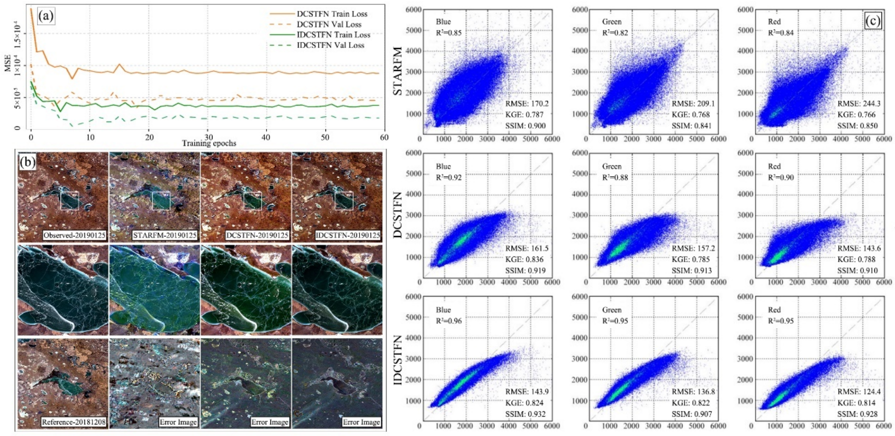

Fig. 9 MODIS-Landsat fusion experiments using IDCSTF. (a) Loss convergence curve; (b) Fusion results from STRAFM, DCSTFN, and IDCSTFN networks on January 25, 2019; (c) Scatter plots of reflectance between the observed image RGB bands and corresponding fused bands, where cyan regions indicate higher density of points.

In the experiment, a dataset containing 21 data groups was used for training and the Adam optimizer was employed to optimize the training process, with Mean Squared Error (MSE) serving as the loss function. The training process demonstrated that the loss value stabilized after 20 epochs of iteration and the IDCSTFN exhibited consistently lower loss values compared to the DCSTFN (**Fig. 9a**). Using the prediction results from January 25, 2019 as a representative case, the difference image generated by STARFM exhibited significantly higher brightness than DCSTFN and IDCSTFN, and revealed anomalous values manifesting as colored stripes (**Fig. 9b**). The distinctions between DCSTFN and IDCSTFN were mainly evident at the edges between water bodies and land, with DCSTFN exhibiting noticeably higher brightness in these regions compared to IDCSTFN. This paper performs image fusion on the RGB channels of MODIS and Landsat. Quantitative analysis through scatter plots of these three bands between observed and fused images demonstrated that the IDCSTFN model outperforms both STARFM and DCSTFN across all bands. Notably, the blue band exhibited slightly higher correlation than the red and green bands, indicating that the blue band is particularly advantageous for fusion in regions dominated by water bodies (**Fig. 9c**).

4.2.2 Interferometric deformation measurement

Synthetic Aperture Radar (SAR) (Bai et al., 2022;Cai et al., 2023) is employed to monitor surface deformation around Chagan Lake, characterized as an active microwave remote sensing system that employs side-looking imaging technology (Gao et al., 2023). The Differential Interferometry SAR (D-InSAR) technique facilitates multiple observations of identical targets through SAR satellites to acquire phase difference information, which enables the calculation of spatial changes relative to the radar. However, D-InSAR encounters limitations in accurate deformation measurement due to atmospheric effects. Persistent Scatterer Interferometric SAR (PS-InSAR) (Ferretti et al., 2001) and Quasi PS-InSAR (QPS-InSAR) (Perissin and Wang, 2011) use Persistent Scatterer (PS) points to establish networks that simulate atmospheric effects, thereby enabling the measurement of surface deformations at millimeter-scale precision (specified in the supplement, PS-InSAR and QPS-InSAR).

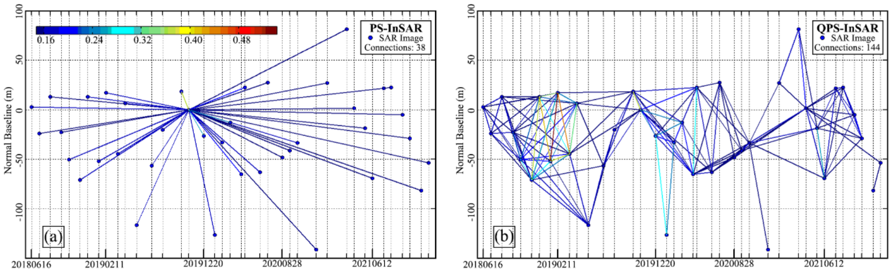

Fig. 10 Topological structure diagram of PS-InSAR and QPS-InSAR.

In the experiment, 39 Sentinel-1 SAR acquisitions from Track 3 were utilized to implement PS-InSAR and QPS-InSAR over the Songnen region (**Table S2**). An image acquired on November 2, 2019 was selected as the master image, and 38 image pairs were generated utilizinga star topology for PS-InSAR (**Fig. 10a**). The maximum baseline length was 141m, remaining less than one-tenth of the critical baseline. For QPS-InSAR processing, the thresholds for coherence, spatial baseline, and temporal baseline were established at 0.148, 108, and 241 respectively, generating 144 interferometric image pairs (**Fig. 10b**).

Acknowledgements

This study was financially supported by the Fundamental Research Funds for the Central Universities (No. B240205012), the Postgraduate Research & Practice Innovation Program of Jiangsu Province (No. KYCX24-837), and the National Natural Science Foundation of China (No. 61771183). We extend our heartfelt gratitude to the use of imagery from the Landsat program, jointly managed by NASA/USGS, MODIS imagery provided by NASA, and Sentinel-1 data from the European Space Agency. Landsat, MODIS, and Sentinel-1 data are freely available for scientific and educational purposes We would like to express our gratitude to GEE platform for its facilities (https://earthengine.google.com/). We would like to express our deep appreciation to the editors and reviewers for their insightful comments and constructive feedback, which significantly improved the quality of our work. Furthermore, we are indebted to all study participants and voluntary contributors, with special thanks to Pinquan Lu, Yitong Zhang, and Wang Wang for their dedicated efforts and support throughout this project.

References

Abuduwaili, J., Issanova, G., and Saparov, G.: Hydrology and limnology of central Asia, Springer, 2018.

Bai, Z., Wang, Y., and Balz, T.: Beijing land subsidence revealed using PS-InSAR with long time series TerraSAR-X SAR data, Remote Sensing, 14, 2529, https://doi.org/10.3390/rs14112529, 2022.

Cai, Y., Li, J., Yang, Q., Liang, D., Liu, K., Zhang, H., Lu, P., and Wang, R.: First demonstration of RFI mitigation in the phase synchronization of LT-1 bistatic SAR, IEEE Transactions on Geoscience and Remote Sensing, 61, https://doi.org/10.1109/TGRS.2023.3310613, 2023.

Chen, J., Wang, C. Y., Tan, H., Rao, W., Liu, X., and Sun, X.: New lakes in the Taklamakan Desert, Geophysical research letters, 39, https://doi.org/10.1029/2012GL053985, 2012.

Chen, Z., Wei, W., Liu, J., Wang, Y., and Chen, J.: Identifying the recharge sources and age of groundwater in the Songnen Plain (Northeast China) using environmental isotopes, Hydrogeology Journal, 19, 163, 2011.

Cook, M. J.: Atmospheric compensation for a landsat land surface temperature product, Rochester Institute of Technology, 2014.

Currell, M. J., Han, D., Chen, Z., and Cartwright, I.: Sustainability of groundwater usage in northern China: dependence on palaeowaters and effects on water quality, quantity and ecosystem health, Hydrological Processes, 26, 4050-4066, https://doi.org/10.1002/hyp.9208, 2012.

Dibike, Y., Prowse, T., Saloranta, T., and Ahmed, R.: Response of Northern Hemisphere lake ‐ ice cover and lake ‐ water thermal structure patterns to a changing climate, Hydrological Processes, 25, 2942-2953, https://doi.org/10.1002/hyp.8068, 2011.

Dong, J., and Bao, W.: Research for the Chagan lake water volume balance differences and unidentified water volume, Jilin Water Resources, 25-27+32, 10.15920/j.cnki.22-1179/tv.2009.01.001, 2009.

Dong, J., and Hu, C.: The water quantity analysis for Qianguo Irrigation water front retreat into Chagan Lake, Jilin Water Resources, 1-4, https://doi.org/10.15920/j.cnki.22-1179/tv.2015.10.001, 2015.

Du, Y., Song, K., Liu, G., Wen, Z., Fang, C., Shang, Y., Zhao, F., Wang, Q., Du, J., and Zhang, B.: Quantifying total suspended matter (TSM) in waters using Landsat images during 1984–2018 across the Songnen Plain, Northeast China, Journal of environmental management, 262, 110334, https://doi.org/10.1016/j.jenvman.2020.110334, 2020.

Ferretti, A., Prati, C., and Rocca, F.: Permanent scatterers in SAR interferometry, IEEE Transactions on geoscience and remote sensing, 39, 8-20, https://doi.org/10.1109/36.898661, 2001.

Gao, Y., Dang, Y., Lu, P., Hou, W., Zhao, F., Wang, B., Yu, W., and Wang, R.: Investigating the dielectric properties of lunar surface regolith fines using Mini-RF SAR data, ISPRS Journal of Photogrammetry and Remote Sensing, 197, 56-70, https://doi.org/10.1016/j.isprsjprs.2023.01.008, 2023.

Ge, Y., Liu, X., Chen, L., Zhang, G., Wu, Y., Yang, X., and Yang, J.: Attribution of lake eutrophication risk to anthropogenic forcing adjacent to the agriculture areas: a case study of Chagan Lake, Environmental Science and Pollution Research, 30, 112159-112172, 2023.

Habermehl, M.: The great artesian basin, Australia, Into the well from which you drink do not throw stones, 82, 2006.

Jiang, Q., and Chen, J.: Analysis on water balance of deep cycle groundwater supplying Tianchi Lake of Changbai Mountain, Water Resources Protection, 31, 7-13, https://doi.org/10.3880/j.issn.1004-6933.2015.05.002, 2015.

Jiang, X.-W., Cherry, J., and Wan, L.: Flowing wells: Terminology, history and role in the evolution of groundwater science, Hydrology and Earth System Sciences, 24, 6001-6019, https://doi.org/10.5194/hess-24-6001-2020, 2020.

Jimenez-Munoz, J. C., Sobrino, J. A., Skoković, D., Mattar, C., and Cristobal, J.: Land surface temperature retrieval methods from Landsat-8 thermal infrared sensor data, IEEE Geoscience and remote sensing letters, 11, 1840-1843, https://doi.org/10.1109/LGRS.2014.2312032, 2014.

Kirillin, G., Leppäranta, M., Terzhevik, A., Granin, N., Bernhardt, J., Engelhardt, C., Efremova, T., Golosov, S., Palshin, N., and Sherstyankin, P.: Physics of seasonally ice-covered lakes: a review, Aquatic sciences, 74, 659-682, https://doi.org/10.1007/s00027-012-0279-y, 2012.

Li, M., Bian, J., Wang, Y., Cui, X., Ding, Y., Sun, X., Wang, F., and Lou, Y.: Identifying interactions of linked irrigated lake-groundwater system by combining hydrodynamic and hydrochemical method, Environmental Science and Pollution Research, 30, 91956-91970, https://doi.org/10.1007/s11356-023-28884-0, 2023.

Li, M., Xie, Y., Dong, Y., Wang, L., and Zhang, Z.: Recent progress on groundwater recharge research in arid and semiarid areas of China, Hydrogeology Journal, 32, 9-30, 2024.

Liao, F., Wang, G., Yang, N., Shi, Z., Li, B., and Chen, X.: Groundwater discharge tracing for a large Ice-Covered lake in the Tibetan Plateau: Integrated satellite remote sensing data, chemical components and isotopes (D, 18O, and 222Rn), Journal of Hydrology, 609, 127741, 2022.

Lingyun, J., Qingliang, W., and Shuangxu, W.: Present-day 3D deformation field of Northeast China, observed by GPS and leveling, Geodesy and Geodynamics, 5, 34-40, https://doi.org/10.3724/SP.J.1246.2014.03034, 2014.

Liu, Q., Guo, X.-d., Wang, C.-q., Lin, N., Zhang, H.-r., Chen, L., and Zhang, Y.: Changes in groundwater resources and their influencing factors in Songnen Plain, China, Journal of Groundwater Science and Engineering, 11, 207-220, https://doi.org/10.26599/JGSE.2023.9280018, 2017.

Liu, X., Zhang, G., Zhang, J., Xu, Y. J., Wu, Y., Wu, Y., Sun, G., Chen, Y., and Ma, H.: Effects of irrigation discharge on salinity of a large freshwater lake: A case study in Chagan Lake, Northeast China, Water, 12, 2112, https://doi.org/10.3390/w12082112, 2020.

Liu, X., Chen, J., Chen, J., and Jin, H.: Shrinking lakes of rift valley system in southern Tibet: Is it the climate?, Science of The Total Environment, 858, 160016, 2023.

Liu, X., Chen, J., Zhang, Q., Zhang, X., Wei, E., Wang, N., Wang, Q., Wang, J., and Chen, J.: Floating on groundwater: Insight of multi-source remote sensing for Qaidam basin, Journal of Environmental Management, 365, 121513, 2024.

Lu, X., Deng, W., and Zhang, S.: Multiple time-scale characteristics of runoff variations in middle reaches of Huolin River and their effects, Chinese Geographical Science, 17, 143-150, https://doi.org/10.1007/s11769-007-0143-5, 2007.

Ma, F., Chen, J., Chen, J., Wang, T., Han, L., Zhang, X., and Yan, J.: Evolution of the hydro-ecological environment and its natural and anthropogenic causes during 1985–2019 in the Nenjiang River basin, Science of The Total Environment, 799, 149256, https://doi.org/10.1016/j.scitotenv.2021.149256, 2021a.

Ma, F., Chen, J., Zhan, L., Zhang, X., Yan, J., and Wang, W.: New insights into water cycle in permafrost region of northern Greater Khingan Mountains, China, Journal of Radioanalytical and Nuclear Chemistry, 330, 631-642, 2021b.

Mallast, U., Gloaguen, R., Friesen, J., Rödiger, T., Geyer, S., Merz, R., and Siebert, C.: How to identify groundwater-caused thermal anomalies in lakes based on multi-temporal satellite data in semi-arid regions, Hydrology and Earth System Sciences, 18, 2773-2787, 2014.

Moore, W. S.: Large groundwater inputs to coastal waters revealed by 226Ra enrichments, Nature, 380, 612-614, 1996.

Perissin, D., and Wang, T.: Repeat-pass SAR interferometry with partially coherent targets, IEEE Transactions on Geoscience and Remote Sensing, 50, 271-280, https://doi.org/10.1109/TGRS.2011.2160644, 2011.

Perissin, D., Wang, Z., and Lin, H.: Shanghai subway tunnels and highways monitoring through Cosmo-SkyMed Persistent Scatterers, ISPRS Journal of Photogrammetry and Remote Sensing, 73, 58-67, http://dx.doi.org/10.1016/j.isprsjprs.2012.07.002, 2012.

Post, V. E., Groen, J., Kooi, H., Person, M., Ge, S., and Edmunds, W. M.: Offshore fresh groundwater reserves as a global phenomenon, Nature, 504, 71-78, 2013.

Roded, R., Aharonov, E., Frumkin, A., Weber, N., Lazar, B., and Szymczak, P.: Cooling of hydrothermal fluids rich in carbon dioxide can create large karst cave systems in carbonate rocks, Communications Earth & Environment, 4, 465 %@ 2662-4435, 2023.

Schilling, O., Nagaosa, K., Schilling, T., Brennwald, M., Sohrin, R., Tomonaga, Y., Brunner, P., Kipfer, R., and Kato, K.: Revisiting Mt Fuji's groundwater origins with helium, vanadium and environmental DNA tracers, Nature Water, 1, 60-73, 2023.

Shen, J., Wu, R., and An, Z.: Characters of the organic $\delta^{13}C$ and paleoenvironment in the section of Dabusu Lake, Journal of Lake Sciences, 10, 8-12, 1998.

Shen, J., Shao, B., Yu, X.-h., Yu, Y., Qi, G., Deng, M., and Zhang, H.: Seismogenic tectonics of the Qian-gorlos earthquake in Jilin Province, China, Earthquake Science, 29, 93-103, https://doi.org/10.1007/s11589-016-0149-0, 2016.

Song, K., Wang, Z., Blackwell, J., Zhang, B., Li, F., Zhang, Y., and Jiang, G.: Water quality monitoring using Landsat Themate Mapper data with empirical algorithms in Chagan Lake, China, Journal of

Applied Remote Sensing, 5, 053506-053506-053516, https://doi.org/10.1117/1.3559497, 2011.

Tan, H., Zhang, Y., Rao, W., Guo, H., Ta, W., Lu, S., and Cong, P.: Rapid groundwater circulation inferred from temporal water dynamics and isotopes in an arid system, Hydrological Processes, 35, e14225, 2021.

Tang, J., Dai, Y., Wang, J., Qu, Y., Liu, B., Duan, Y., and Li, Z.: Study on environmental factors of fluorine in Chagan Lake catchment, Northeast China, Water, 13, 629, https://doi.org/10.3390/w13050629, 2021.

Wang, Q., Wang, X., Xiao, K., Zhang, Y., Luo, M., Zheng, C., and Li, H.: Submarine groundwater discharge and associated nutrient fluxes in the Greater Bay Area, China revealed by radium and stable isotopes, Geoscience Frontiers, 12, 101223, 2021.

Wang, S., Wang, Y., Ran, L., and Su, T.: Climatic and anthropogenic impacts on runoff changes in the Songhua River basin over the last 56 years (1955–2010), Northeastern China, Catena, 127, 258-269, http://dx.doi.org/10.1016/j.catena.2015.01.004, 2015.

Wang, W., Chen, J., Chen, J., Zhan, L., Wang, T., Zhang, Y., and Huang, D.: Basalt and Dune: Critical Factors in Desert Water Resource Development, ACS ES&T Water, https://doi.org/10.1021/acsestwater.4c00001, 2024.

Wang, W., Chen, J., Chen, J. S., Zhang, Y., Liu, X., and Barry, D.: Deep ‑ circulating groundwater from the Tibetan Plateau constructed the Loess Plateau, Geophysical Research Letters, 52, e2024GL110647, 2025.

Wang, Z., Huang, N., Luo, L., Li, X., Ren, C., Song, K., and Chen, J. M.: Shrinkage and fragmentation of marshes in the West Songnen Plain, China, from 1954 to 2008 and its possible causes, International Journal of Applied Earth Observation and Geoinformation, 13, 477-486, https://doi.org/10.1016/j.jag.2010.10.003, 2011.

Wilson, J., and Rocha, C.: Regional scale assessment of Submarine Groundwater Discharge in Ireland combining medium resolution satellite imagery and geochemical tracing techniques, Remote Sensing of Environment, 119, 21-34, 2012.

Wu, G., Fang, H., Li, Z., and Fang, M.: The investigation and study of Qianguo earthquake, 1119, Seismol Res Northeast China, 4, 67-76, https://doi.org/10.13693/j.cnki.cn21-1573.1988.01.013, 1988.

Xu, P., Bian, J., Wu, J., Li, Y., and Ding, F.: Distribution of fluoride in groundwater around Chagan Lake and its risk assessment under the influence of human activities, Water Supply, 20, 2441-2454, https://doi.org/10.2166/ws.2020.135, 2020.

Yang, C., Condon, L. E., and Maxwell, R. M.: Unravelling groundwater–stream connections over the continental United States, Nature Water, 1-10, 2025.

Yong, B., Wang, C.-Y., Chen, J., Chen, J., Barry, D. A., Wang, T., and Li, L.: Missing water from the Qiangtang Basin on the Tibetan Plateau, Geology, 49, 867-872, https://doi.org/10.1130/G48561.1, 2021.

Zhan, L., Chen, J., Xu, Y., Xie, F., and Wang, Y.: Allogenic water recharge of groundwater in the Erenhot wasteland of northern China, Journal of Radioanalytical and Nuclear Chemistry, 311, 2015-2028, http://dx.doi.org/10.1007/s10967-017-5175-4, 2017.

Zhang, B., Song, X., Zhang, Y., Han, D., Tang, C., Yang, L., and Wang, Z.-L.: The relationship between and evolution of surface water and groundwater in Songnen Plain, Northeast China, Environmental Earth Sciences, 73, 8333-8343, 2015.

Zhang, B., Song, X.-F., Zhang, Y.-H., Han, D.-M., Tang, C.-Y., Lihu, Y., and Wang, Z.-L.: The renewability and quality of shallow groundwater in Sanjiang and Songnen Plain, Northeast China, Journal of Integrative Agriculture, 16, 229-238, 10.1016/S2095-3119(16)61349-7, 2017.

Zhang, H., Yu, J., Wang, P., Wang, T., and Li, Y.: Groundwater-fed oasis in arid Northwest China: Insights into hydrological and hydrochemical processes, Journal of Hydrology, 597, 126154, 2021.

Zhang, Y., Chen, J., Chen, J., and Wang, W.: Inter-basin groundwater flow in the Ordos Basin: Evidence of environmental isotope and hydrological investigations, Geoscience Frontiers, 16, 101967, 2025.

Zhu, L., Yan, B., Wang, L., and Pan, X.: Mercury concentration in the muscle of seven fish species from Chagan Lake, Northeast China, Environmental monitoring and assessment, 184, 1299-1310, https://doi.org/10.1007/s10661-011-2041-7, 2012.